RSC Advances

ROYAL SOCIETY OF CHEMISTRY

www.rsc.org/advances

Theoretical study the effect of different substituent on the electronic structures and photophysical properties of phosphorescent Ir(III) complexes

Shuai Zhang,[a] Yanling Si*,[a] and Zhijian Wu*,[b]

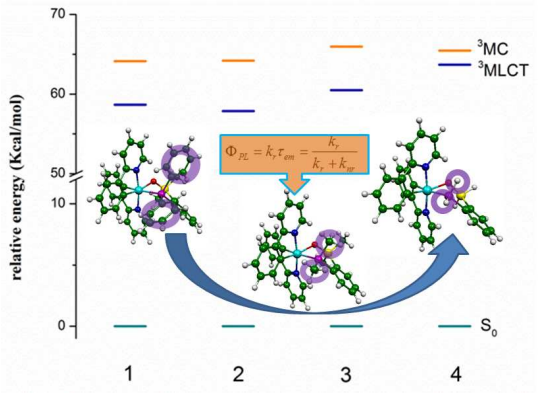

We present the electronic structure, absorption and emission spectra, as well as phosphorescence efficiency of a series of cyclometalated Ir(III) complexes to shed light on the effect of different substituent on the electronic structures and phosphorescence efficiency. The high quantum yield of **1** comapred to **4** is explained based on the S_1-T_1 splitting energy (ΔE_{S1-T1}), the transition dipole moment (μ_{S1}) and energy gap between ^{3}MLCT/π-π* and ^{3}MC d-d states. The designed complexes **2** and **3** are expected to be the potential phosphorescence emitters in OLEDs with high quantum efficiency.

Journal Name

RSCPublishing

ARTICLE

Theoretical study on the effect of different substituents on the electronic structures and photophysical properties of phosphorescent Ir(III) complexes

Cite this: DOI: 10.1039/xoxxoooooox

Received ooth January 2014,
Accepted ooth January 2014

DOI: 10.1039/xoxxoooooox

www.rsc.org/

Shuai Zhang,[a] Yanling Si*,[a] and Zhijian Wu*,[b]

The electronic structure, absorption and emission spectra, as well as phosphorescence efficiency of $(ppy)_2Ir(PPh_2\text{^}SiO)$ (**1**), $(ppy)_2Ir(P(CH_3)_2\text{^}SiO)$ (**2**), $(ppy)_2Ir(PH_2\text{^}SiO)$ (**3**), and $(dfppy)_2Ir(PPh_2\text{^}SiO)$ (**4**) [where ppy=2-phenylpyridne, dfppy=2-(2,4-difluorophenyl)pyridine and $(PR_2\text{^}SiO)$ is an organosilanolate ancillary chelate] were investigated by using the density functional theory (DFT) and time-dependent DFT (TDDF) methods. The results revealed that the subtle differences in geometries and electronic structures result in different spectral properties and the quantum yields. Compared with **1**, the substituent H in **3** leads to obvious red shift in absorption spectra, while the substituent CH_3 leads to a blue shift for **2** in the emission spectra. Moreover, the S_1-T_1 splitting energy ($\Delta E_{S1\text{-}T1}$), the transition dipole moment (μ_{S1}, transition from $S_0 \rightarrow S_1$) and the energy gap between the metal-to-ligand charge transfer ^{3}MLCT/π-π* and metal-centered ^{3}MC/d-d states ($\Delta E_{MC\text{-}MLCT}$) were also calculated. It was found that the designed complexes **2** and **3** have smaller $\Delta E_{S1\text{-}T1}$, larger μ_{S1} and $\Delta E_{MC\text{-}MLCT}$, which make them having higher quantum yield compared with the experimentally synthesized complexes. Therefore, they are expected to be the potential candidates as the emitting materials with high quantum yield.

1 Introduction

As phosphorescent materials, transition metal Ir complexes have attracted a lot of attention, especially in the application of organic light-emitting diodes (OLEDs). Many complexes with high quantum efficiency have been synthesized experimentally. These successful applications are due to the following reasons. The metal Ir is a heavy atom with large spin-orbit coupling. Meanwhile, Ir(III) complexes have high thermal stability, relatively short excited-state lifetime, high photo luminescence efficiency and good emission wavelength tunability. [1-4]

During the past years, numerous red and green phosphorescent Ir(III) complexes with high efficiency have been reported. [5, 6] Besides these two colors, in the visible range, the blue light emitters are also important for white light emitting devices. [7-12] Molecular orbitals, in particular the highest occupied molecular orbital (HOMO) and the lowest unoccupied molecular orbital (LUMO), are important quantities in elucidating both the spectral properties and luminous efficiency. In order to obtain blue-emitting materials energy gap should be large.

It is reported that the efficiency of $Ir(ppy)_3$ can reach 80%.[13] Therefore, a lot of research efforts have been done to find the way to improve the efficiency of other Ir(III) cyclometalated complex for OLEDs application. In the past 10 years, to find out the complexes with 100% internal quantum efficiency, a lot of heteroleptic Ir(III) phosphor complexes with the ancillary ligand derived from the carbanion, have been studied, and it has been found that its efficiency can reach 100%. [14] However, the relationship between structures and spectra is still a major

problem. Reliability and accuracy of the modern computational methods have been widely recognized. Our work is to theoretically provide specific information on the electronic structures and spectral properties, as well as explore the effect of different substituents on the photophysical properties of the studied complexes.

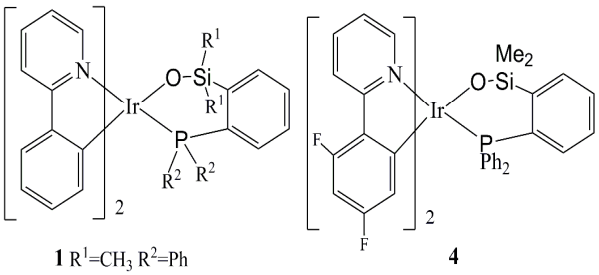

1 R^1=CH_3 R^2=Ph
2 R^1=CH_3 R^2=CH_3
3 R^1=H R^2=H

4

Fig. 1 Schematic structures of the complexes **1**–**4**.

Recently, Zhang *et al.* reported Ir(III) complex $(ppy)_2Ir(PPh_2$^SiO) (**1**) and $(dfppy)_2Ir(PPh_2$^SiO) (**4**) [15] (Fig. 1) (where ppy=2-phenylpyridne, dfppy=2-(2,4-difluorophenyl)pyridine and (PR_2^SiO) is an organosilanolate ancillary chelate). They have a new class of PR_2^SiO chelate, which should provide different properties from those of previously discussed ancillary ligands. Highly intensive luminescence was observed for complexes **1** and **4** with λ_{max} located at 520 nm and 499 nm. However, the experimental quantum yield of **1** (0.90) is much larger than that of **4** (0.59). Meanwhile, the recent report indicates that material with fluorine substituent is harmful for the longevity of OLEDs. [16] From this point of view, the complex **1** is would be more superior than **4**. Based on complex **1** without fluorine substituent, we designed complexes $(ppy)_2Ir(P(CH_3)_2$^SiO) (**2**) and $(ppy)_2Ir(PH_2$^SiO) (**3**) (Fig. 1), aiming at exploring the effects of different substituents on the electronic structures and optoelectronic properties of these Ir(III) complexes.

2 Computational details

The ground state and the lowest-lying triplet excited state geometries for each complex were optimized by using the density functional theory (DFT) [17] with the hybrid-type Perdew-Burke-Ernzerhof exchange correlation functional (PBE0) and the unrestricted PBE0 (UPBE0), [18] respectively, which have been proved to be particularly efficient and accurate for the calculation of transition metal complexes and organic dyes. [19] There were no symmetry constraints on these complexes. The calculated vibrational frequencies for the studied complexes indicate that there was no imaginary frequency on the optimized geometries, which means that the geometries are on the minimum on the potential energy surface. Single-point calculations were performed at the optimized ground-state geometries of these complexes. Besides, the electronic configurations of ^{3}MC d-d states were calculated following the literature methodology, [20, 21] in which optimization starts with a distorted molecular geometry by large elongating the metal-ligand bonds. To obtain the absorption and emission spectra, time dependent DFT (TD-DFT) calculations [22] associated with the polarized continuum model (PCM) [23] in dichloromethane (CH_2Cl_2) media, were performed on the basis of the optimized ground- and lowest triplet excited-state equilibrium geometries. Due to the problem of TDDFT in calculating the charge transfer excited states, [24] one should be cautious in selecting a suitable functional in predicting the emission spectra. Herein, four different functionals (PBE0, B3LYP, M052X and M062X) were performed to assess the effect of different DFT functionals on the emission spectra of **1** and **4**. The B3LYP functional has been used widely to study the excited states of various compounds, however it sometimes fails to describe the charge transfer excitations.[25] The PBE0 functional has been shown to improve the accuracy of excitation energies and charge transfer bands in metal complexes for both gas phase and solution calculations.[26,18c] Recent studies show that M052X and M062X functionals can well describe charge transfer excitations.[27] Our results indicated that M052X is more accurate in reproducing the experimental dada (Table S1, Supporting Information). Therefore, it is selected in the calculation of emission spectra.

Considering large numbers of electrons, the LANL2DZ basis set 28 was employed on the Ir atom, while the 6-31G* [29] basis set was used on C, H, F, N, O, P and Si atoms in the gradient optimizations. A relativistic effective core potential (ECP) on Ir

replaces the inner core electrons, hence leaving the outer core $5s^25p^6$ and $5d^6$ as the valence electrons of Ir(III). These basis sets have been proved to be reliable for cyclometalated Ir(III) complexes. [30] All calculations were performed with the Gaussian 09 package. [31] GaussSum 2.2.5 program [32] was used for the distribution of the total density-of-state analysis as well as UV/Vis spectra analysis. The pictorial representations of the structures and molecular orbital were generated using Molekel 4.3. [33]

3 Result and discussion

3.1 Molecular Geometries in Ground and Excited States

The optimized geometry parameters of the studied complexes in singlet ground state (S_0) and triplet excited state (T_1) are shown in Table 1. For S_0, the optimized structure of the studied four complexes is given in Fig. 2.

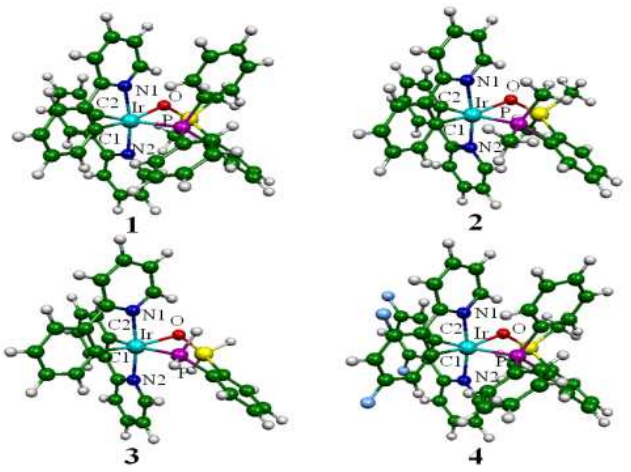

Fig. 2 Optimized ground state structures of the complexes **1**–**4**.

Comparing **1** with **4**, the bond distances between Ir and other atoms are nearly unchanged. Namely, geometry structure is not strongly affected by the addition of fluorination. As for **1** and **2**, the Ir-P bond distances are 2.447 and 2.396 Å, respectively. The existence of CH_3 which size is smaller than phenyl group makes the steric hindrance decreased, strengthening the interaction of Ir atom with $P(CH_3)_2$^SiO group. The Ir-P bond distance of **3,** where phenyl group is replaced by H, is 2.378 Å, smaller than the corresponding values in **1** and **2**. Because the absence of the phenyl group in the PR_2^SiO ligands reduce the steric hindrance significantly, it is easier for electrons in PR_2^SiO ligands and Ir atom to transfer with each other. At the same time, smaller PR_2^SiO ligands result in a tight arrangement of Ir and ligands in **2** and **3**. Compared with **1**, the relatively shorter distance between Ir and ligands in **2** and **3** may facilitate the charge transfer transition between the metal and ligands, eventually enhancing the quantum yield.

The geometry parameters of the studied complexes in the lowest triplet excited states are also listed in Table 1. The calculated Ir–N1 bond distances in **1** and **2** are reduced in T_1 states (Table 1) compared with S_0 states. For Ir – C and Ir – O bond distances, they are also shortened significantly in T_1 states compared with those in S_0 states especially in **2** and **3**, which could increase the interaction between metal and ligands. These differences in structure can attribute to the different electronic structures between S_0 and T_1 states.

Table 1 Main optimized bond distances of the complexes **1**-**4** in the ground and the lowest lying triplet states.

Bond length (Å)	**1**		**2**		**3**		**4**	
	S_0	T_1	S_0	T_1	S_0	T_1	S_0	T_1
Ir-N1	2.040	2.029	2.040	2.031	2.040	2.053	2.039	2.056
Ir-C1	2.004	1.966	1.999	1.971	2.000	1.994	2.001	2.002
Ir-C2	2.020	2.013	2.028	2.014	2.021	1.975	2.018	1.999
Ir-N2	2.070	2.086	2.070	2.086	2.066	2.049	2.070	2.026
Ir-P	2.447	2.528	2.396	2.463	2.378	2.438	2.447	2.479
Ir-O	2.159	2.122	2.167	2.123	2.186	2.170	2.146	2.126

3.2 Frontier molecular orbital analysis

To further study the electronic structure of the studied complexes, we provide the contour plots of the calculated energy of HOMO and LUMO and energy gaps of **1**-**4** in Fig. 3. The detailed information of molecular orbital, including compositions, energies of metal and ligand orbitals are listed in Tables **S2-S5**, respectively, in Supporting Information.

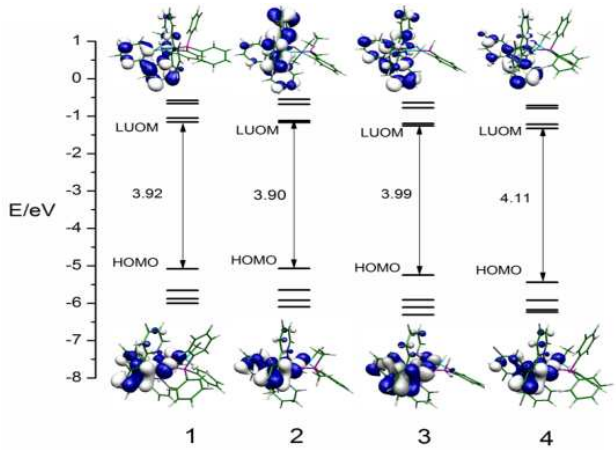

Fig. 3 Contour plots of the HOMO and LUMO and energy gaps for the complexes **1**-**4**.

It is known that the character of the frontier orbital and the HOMO-LUMO energy gap have a great influence on the properties of the complexes. Fig. 3 shows that all complexes have similar FMOs, i.e., HOMO is localized on the d orbital of Ir and π orbital of ppy/dfppy and PR_2^SiO, while the LUMOs are mainly concentrated on the π orbital of ppy (or dfppy). Take **2** as an example. The HOMO is composed of 39% d(Ir), 46% π(ppy), and 14% π($P(CH_3)_2$^SiO), while the LUMO has 96% π*(ppy). The electron densities of the HOMO and LUMO distributions are hardly influenced by different substituents on the ancillary ligands.

However, the different substituents in the PR_2^SiO ligand have a significant effect on the energy levels as shown in Fig. 3. For **2** with CH_3 substituent, the energy of HOMO and LUMO shows a difference of 0.01 eV and -0.01 eV compared with those of **1**. And the energy gap of **2** is narrowed by 0.02 eV. The H substitution in complex **3** stabilizes both HOMO and LUMO energy levels. The decreasing tendency of the HOMO energy level is more significant than that of LUMO in **3**, which results in the increase of the HOMO–LUMO energy gap by 0.07 eV in comparison with that of **1**. Moreover, LUMO and LUMO+1 of **2** and **3** almost degenerate, which can stabilize the excited electrons easily and make **2** and **3** have a better capability in holding the excited electrons, finally result in a better electron transportation process.

3.3 Absorption spectra

TDDFT calculations are widely used to calculate the absorption properties of Ir complexes on the basis of the optimized geometries.[34] Here, the TDDFT/B3LYP method with PCM in CH_2Cl_2 was used to calculate the vertical excitations to discuss the absorption properties of the studied complexes. The calculated results of the complexes **1**-**4** are shown in Table 2. We list the most leading singlet excited states (with larger CI coefficients) and the triplet state associated with their oscillator strengths, dominant orbital excitations and their assignments, along with the corresponding experimental data.

The calculated lowest-lying absorption of **1** at 426 nm, 360 nm and 261 nm are comparable to the experimental values [15] 402 nm, 361 nm and 260 nm, respectively. This means that our calculated absorption data can well reproduce the experimental ones. For complex **1**, the lowest lying singlet-singlet transition primarily comes from HOMO to LUMO (97%) with the absorption band at 426 nm. The HOMO of **1** extends to Ir and ppy ligands with some distribution on the PPh_2^SiO ligand, whereas the LUMO is mainly localized on ppy ligands. Thus, the lowest-lying absorption can be described as metal to ligand charge transfer (MLCT)/intraligand charge transfer (ILCT)/ligand to ligand charge transfer (LLCT). The lowest-lying absorption band of **2** is localized at 426 nm and the excitation of HOMO → LUMO is assigned to d(Ir)+π[ppy+$P(CH_3)_2$^SiO)]→π*(ppy) with the character of MLCT/ILCT/LLCT, which shows that different substituent does not make significant effect on transition character. For complexes **3** and **4**, the lowest-lying absorption is blue-shifted by 12 nm and 23 nm compared with that of **1**.

Table 2 Calculated wavelength (nm)/energies (eV), oscillator strength (*f*) and dominant orbital excitations of the lowest singlet and triplet vertical absorptions for the complexes **1**-**4**, along with experimental data.

	State	λ_{cal}/E	*f*	Configuration (100%)	Nature	Exp.[a]
1	S_1	426/2.91	0.0275	HOMO → LUMO (97%)	MLCT/ILCT/LLCT	402
	S_3	360/3.44	0.0252	HOMO-1 → LUMO (78%)	MLCT/ILCT/LLCT	361
				HOMO-1 → LUMO + 1 (15%)	MLCT/ILCT/LLCT	
	S_{40}	261/4.75	0.1296	HOMO-2 → LUMO + 5 (48%)	LLCT/ILCT	260
				HOMO-2 → LUMO + 6 (14%)	LLCT/ILCT	
	T_1	462/2.68	0.0000	HOMO → LUMO (58%)	MLCT/ILCT/LLCT	
				HOMO → LUMO+1 (20%)	MLCT/ILCT/LLCT	
2	S_1	426/2.91	0.0482	HOMO → LUMO (96%)	MLCT/ILCT/LLCT	
	S_{22}	283/4.38	0.1021	HOMO-2→LUMO+2 (32%)	LLCT/ILCT	
				HOMO-5→LUMO (13%)	MLCT/LLCT/ILCT	
				HOMO-1→LUMO+4 (10%)	MLCT/LLCT/ILCT	
	S_{29}	264/4.70	0.1491	HOMO-2→LUMO+4 (56%)	ILCT/LLCT	
				HOMO→LUMO+6 (12%)	MLCT/LLCT/ILCT	
	S_{31}	260/4.77	0.2091	HOMO-8→LUMO (22%)	MLCT/LLCT/ILCT	
				HOMO-5→LUMO+2 (10%)	MLCT/LLCT/ILCT	
				HOMO-3→LUMO+3 (20%)	MLCT/LLCT/ILCT	
				HOMO→LUMO+6 (12%)	MLCT/LLCT/ILCT	
	T_1	465/2.66	0.0000	HOMO → LUMO (53%)	MLCT/ILCT/LLCT	
				HOMO → LUMO+1 (30%)	MLCT/ILCT/LLCT	
3	S_1	414/3.00	0.041	HOMO→LUMO (97%)	MLCT/LLCT/ILCT	
	S_{19}	281/4.41	0.1669	HOMO-5→LUMO (17%)	ILCT/LLCT	
				HOMO-4→LUMO (17%)	MLCT/LLCT/ILCT	
				HOMO-1→LUMO+3 (17%)	MLCT/LLCT/ILCT	
	S_{28}	259/4.79	0.1342	HOMO-9→LUMO+1(12%)	LLCT/ILCT	
				HOMO-7→LUMO+1(32%)	MLCT/ILCT/LLCT	
				HOMO-3→LUMO+3 (30%)	MLCT/ILCT/LLCT	
	T_1	455/2.72	0.0000	HOMO → LUMO (62%)	MLCT/ILCT/LLCT	
				HOMO → LUMO+1 (11%)	MLCT/ILCT/LLCT	
4	S_1	403/3.07	0.0254	HOMO → LUMO (97%)	MLCT/ILCT/LLCT	385
	S_3	352/3.52	0.0349	HOMO-1 → LUMO (88%)	MLCT/ILCT/LLCT	350
	S_{21}	286/4.34	0.2364	HOMO-4 → LUMO (24%)	ILCT/LLCT	
				HOMO-1 → LUMO + 2 (11%)	MLCT/ILCT/LLCT	
				HOMO-1 → LUMO + 3 (16%)	MLCT/ILCT/LLCT	
				HOMO-1 → LUMO + 4 (15%)	MLCT/ILCT/LLCT	
	T_1	438/2.83	0.0000	HOMO → LUMO (47%)	MLCT/ILCT/LLCT	
				HOMO-1 → LUMO (21%)	MLCT/ILCT/LLCT	

[a] Ref. [15]

From Table 2, in singlet state, the maximum absorption peaks of **1** and **2** are located at 261 and 260 nm, which is nearly the same. For **3** and **4**, the transitions with the largest oscillator strengths are located at 281 and 286 nm, which is slightly red-shifted compared with **1**. On the transition $S_0 \rightarrow T_1$, the absorption band of **1** located at 462 nm is contributed by HOMO → LUMO (58%) and HOMO → LUMO + 1 (20%) transition with the character of MLCT/ILCT/LLCT. The non-negligible MLCT is beneficial for efficient intersystem crossing, and singlet-triplet transitions will lead to the high quantum efficiency for these Ir(III) complexes. Similarly, The calculated lowest-lying triplet absorptions of **2** and **3** are at 465 and 455 nm, respectively, with the main transition HOMO → LUMO and HOMO → LUMO + 1. For **4**, the transition HOMO → LUMO (47%) and HOMO-1 → LUMO (21%) contribute to the 438 nm absorption.

3.4 Emission properties

We used four different density functionals to calibrate the computational method. Experimental results for the complexes of **1** and **4** are compared with the calculated values, which is listed in

Table S1. The calculated lowest emission energies for **1** and **4** at M052X level are localized at 493 and 499 nm, which is close to the experimental values at 499 and 520 nm. For **1**, the calculated values with PBE0, B3LYP, M062X level deviate from experimental values by 42, 43, 44 nm, respectively. The similar situation occurs to **4**. Thus, M052X was selected for the calculation of emission spectra. The calculated phosphorescent emissions of **1**-**4** with M052X level are shown in Table 3.

For **1**, the emission is contributed mainly by HOMO → LUMO transition (65%). According to our calculation, the HOMO is delocalized on Ir (40%), ppy (45%) and PPh_2^SiO ligand (14%), while the LUMO is mainly from ppy (95%). Therefore, this emission can be assigned as MLCT/ILCT/LLCT. For **2** and **3**, there are two transitions contributing to calculated emission, which are HOMO → LUMO and HOMO-1→ LUMO transitions. The HOMO and HOMO-1 are occupied by the d orbital of Ir, ppy and PCH_3^SiO/ PH_2^SiO, while the LUMO is mainly contributed by ppy (95%). The emission can be assigned as MLCT/ILCT with little contribution of LLCT. In addition, the emission of **4** comes from HOMO-1 → LUMO (52%) and HOMO → LUMO (36%) with the mixed characters of MLCT/ILCT/LLCT. From Table 3, we can see that the calculated lowest-energy emissions of **2**-**4** are localized at 488 nm, 497 nm and 493 nm. With the substituent F on dfppy ligand, the emission wavelength of **4** has been blue-shifted slightly compared to complex **1**. For the designed complexes **2** and **3** with the substituents CH_3 and H on PR_2^SiO ligands, a blue-shift is also observed, in particular for **2**.

3.5 The photoluminescent quantum efficiency

The quantum yield Φ_{PL} is linked to the radioactive (k_r) and the nonradioactive (k_{nr}) rate constants by Equation (1), where τ_{em} is the emission decay time.

$$\Phi_{PL} = k_r \tau_{em} = \frac{k_r}{k_r + k_{nr}} \qquad (1)$$

Therefore, larger k_r and smaller k_{nr} would improve quantum yield Φ_{PL}. Theoretically, taking into account only the lowest excited singlet and triplet states, k_r is inversely proportional to the energy difference between the S_1 and T_1 states. The radioactive rate can be approximated by the following: [35, 36]

$$k_r = \gamma \cdot E_{em}^3 \frac{\langle \Psi_{S1} | H_{S0} | \Psi_{T1} \rangle^2 \cdot \mu_{S1}^2}{(\Delta E_{S1-T1})^2} \qquad \gamma = \frac{16\pi^3 10^6 n^3}{3h\varepsilon_0} \qquad (2)$$

In Equation (2), μ_{S1} is the transition electric dipole moment in S_0-S_1 transition, E_{em} represents the emission energy in cm^{-1}, while n, h, and ε_0 are the refractive index, Planck's constant and the permittivity in vacuum, respectively. The orbitals of Ir atom make a great contribution in the excited states through the spin-orbit coupling (SOC) and thus intersystem crossing (ISC). The SOC effects are mainly determined by the following two aspects.

One aspect is the contribution of MLCT in the T_1 state. [37] In the T_1-S_0 transition, the involvement of d(Ir) orbital enhances the first-order SOC, which would lead to the decrease of radiative lifetime and avoid the non-radiative process. [38] In other words, a larger MLCT contribution is beneficial to increase the quantum yield higher. At the same time, the S_1-T_1 energy gap (ΔE_{S1-T1}) is the

Table 3 Calculated phosphorescent emission (in nm) of the complexes **1**-**4** in CH_2Cl_2 media with the TDDFT method, along with experimental values.

	λ_{cal}/E(eV)	Configuration	Character	Exp.[a]
1	499/2.49	HOMO → LUMO (65%)	MLCT/ILCT/LLCT	520
2	488/2.54	HOMO → LUMO (59%)	MLCT/ILCT/LLCT	
		HOMO-1 → LUMO (15%)	MLCT/ILCT/LLCT	
3	497/2.49	HOMO → LUMO (49%)	MLCT/ILCT/LLCT	
		HOMO-1 → LUMO (37%)	MLCT/ILCT/LLCT	
4	493/2.51	HOMO-1 → LUMO (52%)	MLCT/ILCT/LLCT	499
		HOMO → LUMO (36%)	MLCT/ILCT/LLCT	

[a] Ref. [15].

second factor that affects the SOC effects. [39] The $S_1 \rightarrow T_1$ ISC induced by SOC interactions plays an important role in the phosphorescent process. Through Equation (2), we can see that both a decrease of ΔE_{S1-T1} and a larger μ_{S1} will lead to an increase of k_r, which further result to a higher quantum yield. Thus, for enhancing the ISC rate, a small ΔE_{S1-T1} and a large μ_{S1} is necessary, and this would lead to an increased k_r.

The metal-based charge transfer character (MLCT, 100%), the S_1-T_1 calculated energy gaps (ΔE_{S1-T1}), the transition dipole moment and experimental quantum yield are listed in Table 4. From Table 4, we can see that the calculated MLCT contribution of **1** and **4** are 36.00% and 36.36%. The MLCT contribution of **4** is almost equal to that of **1**, while the quantum yield of **4** (0.59) is lower than that of **1** (0.90). Thus, for complexes **1** and **4**, the MLCT contribution is not the critical factor for the quantum yield.

For **1** and **4**, the calculated ΔE_{S1-T1} are 0.769 and 1.008 eV, and the calculated μ_{S1} are 0.3855, 0.3372 D, respectively. The ΔE_{S1-T1} of **1** is smaller than that of **4**, while the μ_{S1} of **1** is slightly larger than that of **4**. This may explain the different Φ_{PL} observed in experiment. The designed complexes **2** and **3** have larger μ_{S1} and smaller ΔE_{S1-T1} than those of **4**. Therefore, we predict that they can be good candidates with higher k_r. From the discussion above, the radioactive decay rate k_r are related to many factors. Larger MLCT contribution, a smaller ΔE_{S1-T1} and larger μ_{S1} are needed. Beside these factors, there are also other factors that might play an important role for a high quantum yield.

Table 4 The metal-based charge transfer character (MLCT, %), singlet-triplet splitting (ΔE_{S1-T1} in eV) and the transition dipole moment in $S_0 \rightarrow S_1$ transition (μ_{S1} in Debye), along with experimental quantum yield Φ_{PL}

Parameter	**1**	**2**	**3**	**4**
MLCT (%)	36.00	28.29	32.30	36.36
μ_{S1}	0.3855	0.6758	0.5587	0.3372
ΔE_{S1-T1}	0.769	0.730	0.838	1.008
Φ_{PL} (%)	0.90[a]			0.59[a]

[a] Ref. [15].

In transition-metal complexes, the higher-lying metal-centered (3MC/d-d) triplet excited states are regarded as one of the most from T_1. [40] By thermal activation, the lowest metal-to-ligand charge transfer (^{3}MLCT/π-π^*) excited state can be changed to metal-centered (^{3}MC/d-d) state, whose lifetime is relatively short. [41, 42] During this process, there is no photochemistry occurs and the conversion is very fast and irreversible. The energy gap between ^{3}MLCT/π-π* and ^{3}MC/d-d states plays an important role in ^{3}MLCT-^{3}MC conversion. [43, 44] We show the calculated results in Fig. 4 with the normalized S_0 levels.

Theoretically, a larger separation between ^{3}MLCT/π-π* and ^{3}MC/d-d states can bring a smaller k_{nr} and thus a higher phosphorescence quantum yield. From Fig. 4, the separation in energy between ^{3}MLCT/π-π* and ^{3}MC /d-d states of **2** is larger than that of **1**. This suggests that the k_{nr} of **2** could be smaller than the one of **1**. Both ^{3}MLCT and ^{3}MC of **3** increase compared with **1**. However, the energy gap ^{3}MLCT/π-π* and ^{3}MC /d-d states of **3** is almost the same with that of **1**, but larger than **4**. Then, the order of k_{nr} would be $k_{nr2} < k_{nr3} \approx k_{nr1} < k_{nr4}$. Through the above analysis, complexes **2** and **3** have a relatively larger k_r and smaller k_{nr}. This means that they would have higher quantum yield.

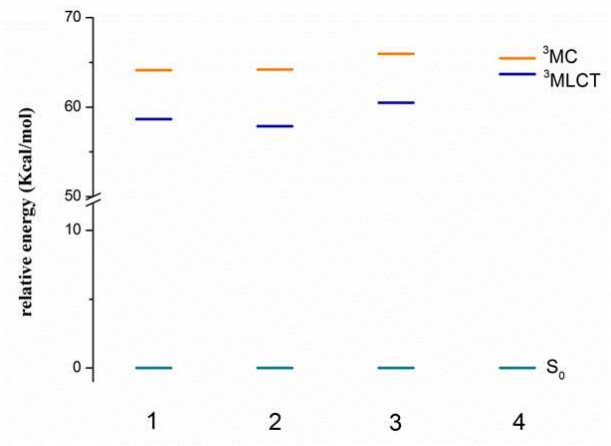

Fig. 4 Energy level diagram of the complexes **1**-**4** in ^{3}MLCT and ^{3}MC excited states, respectively, along with the normalized S_0 levels.

4 Conclusions

DFT/TDDFT calculations have been conducted to investigate the influence on the photophysical properties by introduction of different substituents. The following conclusions can be made. (1) The energy levels of the FMOs are influenced by molecular volume size of PR_2^OSi. (2) Compared with the parent complex **1**, the lowest-lying absorption bands of **2** is nearly the same, while it is red-shifted for **3**. (3) The emission of **2** is blue-shifted**,** but nearly the same for **3**. (4) The $\Delta E_{S1\text{-}T1}$ of **1** is smaller than that of **4**, and the μ_{S1} of **1** is larger than the one of **4**, which could explain the different Φ_{PL} observed in experiment. The complexes **2** and **3** have smaller $\Delta E_{S1\text{-}T1}$and larger μ_{S1}. Therefore, we predicted that they may be promising complexes with higher k_r. On the other hand, the separations in energy between ^{3}MLCT/π-π* and ^{3}MC /d-d states of **2** and **3** are relatively larger. Thus, they could have higher quantum yield. We hope that our studies will stimulate the further investigation in designing highly efficient phosphorescent materials.

Acknowledgements

The authors thank the financial support from the National Natural Science Foundation of China (Grant Nos. 21273219, 21221061, 21203174), Natural Science Foundation of Jilin Province (20140101045JC) and computing time from the High Performance Computing Center of Jilin University, China.

Notes and references

[a]College of Resource and Environmental Science, Jilin Agricultural University, Changchun, 130118, P.R. China

[b]State Key Laboratory of Rare Earth Resource Utilization, Changchun Institute of Applied Chemistry, Chinese Academy of Sciences, Changchun, 130022, P. R. China.

*Corresponding author. Email: siyl400@nenu.edu.cn; zjwu@ciac.ac.cn

† Electronic Supplementary Information (ESI) available: Tables: (S1) Calculated phosphorescent emission wavelength (nm)/energies (eV) of the complexes **1** and **4** in CH_2Cl_2 media with the TDDFT method at the B3LYP, M062X, M052X and PBE0 level, respectively, together with the experimental values. (S2-S5) Molecular orbital composition (%) of complexes**1**–**4** in the ground state; (S6-S9) The xyz coordinates for the optimized S_0 structures for **1**–**4**. See DOI: 10.1039/b000000x/

1 (a) W. Y. Wong, G. J. Zhou, X. M. Yu, H. S. Kwok and B. Z. Tang, *Adv. Funct. Mater.*, 2006, **16**, 838-846; (b) Z. Q. Chen, Z. Q. Bian and C. H. Huang, *Adv. Mater.*, 2010, **22**, 1534-1539; (c) C. Ulbricht, B. Beyer, C. Friebe, A. Winter and U. S. Schubert, *Adv. Mater.*, 2009, **21**, 4418-4441; (d) Y. You and S. Y. Park, *Dalton Trans.*, 2009, 1267-1282; (e) X. Li, Q. Zhang, Y. Q. Tu, H. Agren and H. Tian, *Phys. Chem. Chem. Phys.*, 2010, **12**, 13730-13736.

2 X. S. Zeng, M. Tavasli, I. F. Perepichka, A. S. Batsanov, M. R. Bryce, C. J. Chiang, C. Rothe and A. P. Monkman, *Chem. -Eur. J.*, 2008, **14**, 933-946.

3 L. He, L. Duan, J. Qiao, R. J. Wang, P. Wei, L. D. Wang and Y. Qiu, *Adv. Funct. Mater.*, 2008, **18**, 2123-2131.

4 (a) Q. Zhao, S. J. Liu, M. Shi, C. M. Wang, M. X. Yu, L. Li, F. Y. Li, T. Yi and C. H. Huang, *Inorg. Chem.*, 2006, **45**, 6152-6160; (b) S. J. Liu, Q. Zhao, R. F. Chen, Y. Deng, Q. L. Fan, F. Y. Li, L. H. Wang, C. H. Huang and W. Huang, *Chem.-Eur. J.*, 2006, **12**, 4351-4361; (c) Q. Zhao, L. Li, F. Y. Li, M. X. Yu, Z. P. Liu, T. Yi and C. H. Huang, *Chem. Commun.*, 2008, 685-687; (d) S. J. Liu, Q. Zhao, B. X. Mi and W. Huang, *Adv. Polym. Sci.*, 2008, **212**, 125-144; (e) Q. Zhao, S. J. Liu and W. Huang, *Macromol. Rapid Commun.*, 2010, **31**, 794-807; (f) H. F. Shi, Y. Nakai, S. J. Liu, Q. Zhao, Z. F. An, T. Tsuboi and W. Huang, *J. Phys. Chem. C*, 2011 **115**, 11749-11757.

5 C. Adachi, M. A. Baldo, S. R. Forrest and M. E. Thompson, *Appl. Phys. Lett.*, 2000, **77**, 904-906.

6 C. Adachi, M. A. Baldo, S. R. Forrest, S. Lamansky, M. E. Thompson and R. C. Kwong, *Appl. Phys. Lett.*, 2001, **78**, 1622-1624.

7 S. C. Yu, C. C. Kwok, W. K. Chan, C. M. Che, *Adv. Mater.*, 2003, **15**, 1643-1647.

8 C. M. Che, S. C. Chan, H. F. Xiang, M. C. W. Chan, Y. Liu, Y. Wang, *Chem. Commun.*, 2004, 1484-1485.

9 B. W. D'Andrade, R. J. Holmes, S. R. Forrest, *Adv. Mater.*, 2004, **16**, 624-628.

10 P. Coppo, M. Duati, V. N. Kozhevnikov, J. W. Hofstraat, L. De. Cola, *Angew. Chem. Int. Ed.*, 2005, **44**, 1806-1810.

11 P. T. Furuta, L. Deng, S. Garon, M. E. Thompson, J. M. J. Frechet, *J.*

Am. Chem. Soc., 2004, **126**, 15388-15389.

12 M. Sun, B. Niu, J. P. Zhang, *Theor. Chem. Acc.*, 2008, **119**, 489-500.

13 M. A. Baldo, M. E. Thompson, S. R. Forrest, *Nature.*, 2000, **403**, 750-753.

14 K. Dedeian, J. Shi, N. Shepherd, E. Forsythe, D. C. Morton, *Inorg. Chem.*, 2005, **44** , 4445-4447.

15 F. S. Zhang, L. D. Wang, S. H. Chang, K. L. Huang, Y. Chi, W. Y. Hung, C. M. Chen, G. H. Lee and P. T. Chou, *Dalton Trans.*, 2013, **42**, 7111-7119.

16 V. Sivasubramaniam, F. Brodkorb, S. Hanning, H. P. Loebl, V. van. Elsbergen, H. Boerner, U. Scherf and M. Kreyenschmidt, *J. Fluorine Chem.*, 2009, **130**, 640-649.

17 E. Runge and E. K. U. Gross, *Phys. Rev. Lett.*, 1984, **52**, 997-1000.

18 (a) J. P. Perdew, K. Burke and M. Ernzerhof, *Phys. Rev. Lett.*, 1996, **77**, 3865-3868; (b) J. P. Perdew, K. Burke and M. Ernzerhof, *Phys. Rev. Lett.*, 1997, **78**, 1396-1396; (c) C. Adamo and V. Barone, *J. Chem. Phys.*, 1999, **110**, 6158-6170.

19 (a) T. Liu, B. H. Xia, Q. C. Zheng, X. Zhou, Q. J. Pan and H. X. Zhang, *J. Comput. Chem.*, 2010, **31**, 628-638; (b) I. Ciofini, P. P. Laine, F. Bedioui and C. Adamo, *J. Am. Chem. Soc.*, 2004, **126**, 10763-10777; (c) I. Ciofini, P. P. Laine, F. Bedioui C. A. Daul and C. Adamo, *C. R. Chim.*, 2006, **9**, 226-229; (d) D. Jacquemin, E. A. Perpete, G. Scalmani, M. J. Frisch, I. Ciofini and C. Adamo, Chem. Phys. Lett., 2006, **421**, 272-276; (e) I. Ciofini, P. P. Laine, M. Zamboni, C. A. Daul, V. Marvaud and C. Adamo, *Chem. -Eur. J.*, 2007, **13**, 5360-5377; (f) Y. L. Si, Y. Q. Liu, X. C. Qu, Y. Wang and Z. J. Wu, *Dalton Trans.*, 2013, **42**, 14149-14157.

20 M. Abrahamsson, M. J. Lundqvist, H. Wolpher, O. Johansson, L. Eriksson, J. Bergquist, T. Rasmussen, H. C. Becker, L. Hammarstrom and P. O. Norrby, *Inorg. Chem.*, 2008, **47**, 3540-3548.

21 J. Y. Hung, C. H. Lin, Y. Chi, M. W. Chung, Y. J. Chen, G. H. Lee, P. T. Chou, C. C. Chen and C. C. Wu, *J. Mater. Chem.*, 2010, **20**, 7682-7693.

22 (a) J. Autschbach, T. Ziegler, S. J. A. Gisbergen and E. J. Baerends, *J. Chem. Phys.*, 2002, **116**, 6930-6940; (b) T. Helgaker and P. Jørgemsen, *J. Chem. Phys.*, 1991, **95**, 2595-2601; (c) K. L. Bak, P. Jørgemsen, T. Helgaker, K. Rund and H. J. A. Jensen, *J. Chem. Phys.*, 1993, **98**, 8873-8887.

23 (a) E. Cancès, B. Mennucci and J. Tomasi, *J. Chem. Phys.*, 1997, **107**, 3032-3041; (b) M. Cossi, V. Barone, B. Mennucci and J. Tomasi, *Chem. Phys. Lett.*, 1998, **286**, 253-260; (c) B. Mennucci and J. Tomasi, *J. Chem. Phys.*, 1997, **106**, 5151-5198.

24 (a) A. Dreuw, J. L. Weisman and M. Head-Gordon, *J. Chem. Phys.*, 2003, **119**, 2943-2946; (b) A. Dreuw and M. Head-Gordon, *J. Am. Chem. Soc.*, 2004, **126**, 4007-4016.

25 (a) A. D. Becke, *J. Chem. Phys.*, 1993, **98**, 5648-5652; (b) C. T. Lee, W. T. Yang and R. G. Parr, *Phys. Rev. B*, 1988, **37**, 785-789; (c) A. Dreuw and M.Head-Gordon, *Chem. ReV.,* 2005, **105**, 4009-4037; (d) Y. Zhao and D. G. Truhlar, *J. Phys. Chem. A*, 2006, **110**, 13126-13130.

26 C. Adamo and V. Barone, *Chem. Phys. Lett.,* 1999, **314**, 152.

27 (a) Y. Zhao, N.E. Schultz, D.G. Truhlar, *J. Chem. Phys.* 2005, **123**, 194101; (b) Y. Zhao, N. E. Schultz and D. G. Truhlar, *J. Chem. Theory Comput.*, 2006, **2**, 364-382; (c) Y. Zhao and D. G. Truhlar, *Theor. Chem. Acc.*, 2008, **120**, 215-241; (d) D. Jacquemin, E. A. Perpète, I. Ciofini, C. Adamo, R.Valero, Y. Zhao and D. G. Truhlar, *J. Chem. Theory. Comput.*, 2010, **6**, 2071−2085.

28 (a) P. J. Hay and W. R. Wadt, *J. Chem. Phys.*, 1985, **82**, 270-283; (b) P. J. Hay and W. R. Wadt, *J. Chem. Phys.*, 1985, **82**, 299-310.

29 P. C. Hariharan and J. A. Pople, *Mol. Phys.*, 1974, **27**, 209-214.

30 X. N. Li, Z. J. Wu, Z. J. Si, H. J. Zhang, L. Zhou and X. J. Liu, *Inorg. Chem.*, 2009, **48**, 7740-7749.

31 M. J. Frisch, G. W. Trucks, H. B. Schlegel, G. E. Scuseria, M. A. Robb, J. R. Cheeseman, G. Scalmani, V. Barone, B. Mennucci, G. A. Petersson, H. Nakatsuji, M. Caricato, X. Li, H. P. Hratchian, A. F. Izmaylov, J. Bloino, G. Zheng, J. L. Sonnenberg, M. Hada, M. Ehara, K. Toyota, R. Fukuda, J. Hasegawa, M. Ishida, T. Nakajima, Y. Honda, O. Kitao, H. Nakai, T. Vreven, J. A. Montgomery, Jr. J. E. Peralta, F. Ogliaro, M. Bearpark, J. J. Heyd, E. Brothers, K. N. Kudin, V. N. Staroverov, T. Keith, R. Kobayashi, J. Normand, K. Raghavachari, A. Rendell, J. C. Burant, S. S. Iyengar, J. Tomasi, M. Cossi, N. Rega, J. M. Millam, M. Klene, J. E. Knox, J. B. Cross, V. Bakken, C. Adamo, J. Jaramillo, R. Gomperts, R. E. Stratmann, O. Yazyev, A. J. Austin, R. Cammi, C. Pomelli, J. W. Ochterski, R. L. Martin, K. Morokuma, V. G. Zakrzewski, G. A. Voth, P. Salvador, J. J. Dannenberg, S. Dapprich, A. D. Daniels, O. Farkas, J. B. Foresman, J. V. Ortiz, J. Cioslowski and D. Fox, J. *Gaussian 09*, Revision B.01; Gaussian, Inc., Wallingford, CT,

2010.

32 N. M. O'Boyle, A. L. Tenderholt and K. M. Langner, *J. Comput. Chem.*, 2008, **29**, 839-845.

33 P. Flükiger, H. P. Lüthi, S. Portmann and J. Weber, MOLEKEL 4.3 Swiss Center for Scientific Computing, Manno. Switzerland, 2000; S. Portmann and H. P. Luthi, Chimia, 2000, **54**, 766-770.

34 (a) H. R. Tsai, K. Y. Lu, S. H. Lai, C. H. Fan, C. H. Cheng, and I. C. Chen, *J. Phys. Chem. C*, 2011, **115**, 17163-17174; (b) P. Jeffrey Hay, *J. Phys. Chem. A*, 2002, **106**, 1634-1641; (c) A. R. G. Smith, M. J. Riley, S. C. Lo, P. L. Burn, I. R. Gentle, and B. J. Powell, *Phys. Rev. B*, 2011, **83**, 041105; (d) Y. L. Si, Y. Q. Liu, G. Gahungu, X. C. Qu and Z. J. Wu, *Mol. Phys.*, 2013, **111**, 3716-3725.

35 S. Haneder, E. Da Como, J. Feldmann, J. M. Lupton, C. Lennartz, P. Erk, E. Fuchs, O. Molt, I. Munster, C. Schildknecht and G. Wagenblast, *Adv. Mater.*, 2008, **20**, 3325-3330.

36 N. Turro. Modern Molecular Photochemistry, University Science Books, Palo Alto, USA, 1991.

37 J. Li, P. I. Djurovich, B. D. Alleyne, M. Yousufuddin, N. N. Ho, J. C. Thomas, J. C. Peters, R. Bau and M. E. Thompson, *Inorg. Chem.*, 2005, **44**, 1713-1727.

38 C. H. Yang, Y. M. Cheng, Y. Chi, C. J. Hsu, F. C. Fang, K. T. Wong, P. T. Chou, C. H. Chang, M. H. Tsai and C. C. Wu, *Angew. Chem. Int. Ed.*, 2007, **46**, 2418-2421.

39 I. Avilov, P. Minoofar, J. Cornil and L. De Cola, *J. Am. Chem. Soc*., 2007, **129**, 8247-8258.

40 (a) G. Treboux, J. Mizukami, M. Yabe, S. Nakamura, *Chem. Lett.*, 2007, **36**, 1344-1345; (b) F. Alary, J. L. Heully, L. Bijeire, P. Vicendo, *Inorg. Chem.*, 2007, **46**, 3154-3165; (c) J. Van Houten, R. J. Watts, *J. Am. Chem. Soc.*, 1976, **98**, 4853-4858; (d) T. Sajoto, I. Djurovich, A. B. Tamayo, J. Oxgaard, W. A. Goddard, M. E. Thompson, *J. Am. Chem. Soc.*, 2009, **131**, 9813-9822; (e) Roundhill, D. M. Photochemistry and Photophysics of Metal Complexes, Plenum Press: New York , 1994.

41 Kalyanasundaram, K. Photochemistry of Polypyridine and Porphyrin Complexes, Academic Press: London, 1992.

42 T. J. Meyer, *Pure Appl. Chem.*, 1986, **58**, 1193-1206.

43 C. H. Lin, Y. Y. Chang, J. Y. Hung, C. Y. Lin, Y. Chi, M. W. Chung, C. L. Lin, P. T. Chou, G. H. Lee, C. H. Chang and W. C. Lin, *Angew. Chem. Int. Ed.*, 2011, **50**, 3182-3186.

44 J. Y. Hung, C. H. Lin, Y. Chi, M. W. Chung, Y. J. Chen, G. H. Lee, P. T. Chou, C. C. Chen and C. C. Wu, *J. Mater. Chem.*, 2010, **20**, 7682-7693.

